*International Conference on Mathematics, Computational Methods & Reactor Physics (M&C 2009)*
Saratoga Springs, New York, May 3-7, 2009, on CD-ROM, American Nuclear Society, LaGrange Park, IL (2009)

# FOURIER ANALYSIS OF CELL-WISE BLOCK-JACOBI SPLITTING IN TWO-DIMENSIONAL GEOMETRY

**Massimiliano Rosa, James S. Warsa and Timothy M. Kelley**
Los Alamos National Laboratory
P.O. Box 1663, MS K784, Los Alamos, NM 87545, USA
maxrosa@lanl.gov; warsa@lanl.gov; tkelley@lanl.gov

## ABSTRACT

A Fourier analysis is conducted in two-dimensional (2D) geometry for the discrete ordinates ($S_N$) approximation of the neutron transport problem solved with Richardson iteration (Source Iteration) using the cell-wise Block-Jacobi (BJ) algorithm. The results of the Fourier analysis show that convergence of cell-wise BJ can degrade, leading to a spectral radius equal to 1, in problems containing optically thin cells. For problems containing cells that are optically thick, instead, the spectral radius tends to 0. Hence, in the optically thick-cell regime, cell-wise BJ is rapidly convergent even for problems that are scattering dominated, with a scattering ratio $c$ close to 1.

*Key Words*: neutral particle transport, Fourier analysis, Block-Jacobi, Finite Element Methods

## 1. INTRODUCTION

Computational methods for particle transport are very demanding, consuming the bulk of computational resources in a range of multi-physics simulations, including astrophysics calculations and nuclear reactor design. Current transport methods have evolved incrementally in response to advances in hardware technology. This picture, though, may soon change dramatically. It is understood by the scientific computing community that parallel, advanced heterogeneous computing architectures may become the machines of choice for large scale computing in the future. The new machines have different processors and communication layers at different levels in their architecture, with different processing characteristics and capabilities at each level. Heterogeneous computing platforms, like the Roadrunner [1] machine being deployed at Los Alamos National Laboratory, require the development of new transport methods, or to reconsider previously discarded methods, in order to make full use of their capabilities.

In this paper we conduct a study of the stability and convergence properties of the cell-wise BJ algorithm, targeted at Roadrunner's heterogeneous architecture. Fourier analysis is traditionally used to study transport iteration schemes in a homogeneous infinite medium. In fact, it is a valuable tool to understand the behavior of the iteration error modes of various iterative schemes. Therefore, we conduct a Fourier analysis for the $S_N$ approximation of the steady-state one-group transport problem solved with Richardson iteration using cell-wise BJ. The spatial discretization is a Discontinuous Finite Element Method (DFEM) [2], specialized to triangular cells, and the scattering is assumed to be isotropic. The analysis is verified with results from a 2D transport code that implements cell-wise BJ on available parallel, homogeneous computing architectures. Further research is envisioned to port the code on Roadrunner's heterogeneous architecture.

## 2. FOURIER ANALYSIS OF CELL-WISE BJ IN 2D GEOMETRY

### 2.1. Cell-Wise Block-Jacobi Splitting

The homogeneous transport equation is written, for isotropic scattering, in compact operator notation:

$$L\psi = S\phi, \tag{1}$$

where $L$ represents the "streaming plus total interaction" operator, $S$ is the scattering operator, $\psi$ is the angular flux and $\phi$ is the scalar flux. Furthermore, the scalar flux is the integral of the angular flux over all angles:

$$\phi = D\psi, \tag{2}$$

where $D$ is the "discrete-to-moment" operator.

In the cell-wise BJ algorithm, the incoming angular fluxes at the boundaries between a computational cell and its neighboring cells are "lagged" from the previous iteration. Accordingly, we split the "streaming plus total interaction" operator into $L_c$ (cell's interior) and $L_b$ (cell's boundaries):

$$L = L_c + L_b. \tag{3}$$

The cell-wise BJ algorithm is then implemented through the following iteration scheme:

$$\psi^{(\ell+1)} = -\left(L_c - SD\right)^{-1} L_b \psi^{(\ell)}, \tag{4}$$

where $\ell \geq 0$ is the iteration index. Consequently, a formulation of the transport problem in terms of angular fluxes only is obtained. Not only is this formulation convenient in order to devise a Fourier analysis for cell-wise BJ, but it is actually utilized in its practical implementation. In fact, apart from the "lagging" of the contributions at a cell's boundaries, the "full" transport operator is locally inverted on each computational cell in order to compute the angularly and spatially discretized angular fluxes in the present iteration. It is hoped that such formulation may result in an arithmetic intensive algorithm for radiation transport particularly suited for large scale computing on Roadrunner's parallel, heterogeneous computing architecture.

### 2.2. Fourier Analysis

The equations representing the fixed-source-free 2D DFEM spatial discretization of the $S_N$ approximation to Eq. (1) are written for the system of four triangular cells over a Cartesian element sketched in Fig. 1.

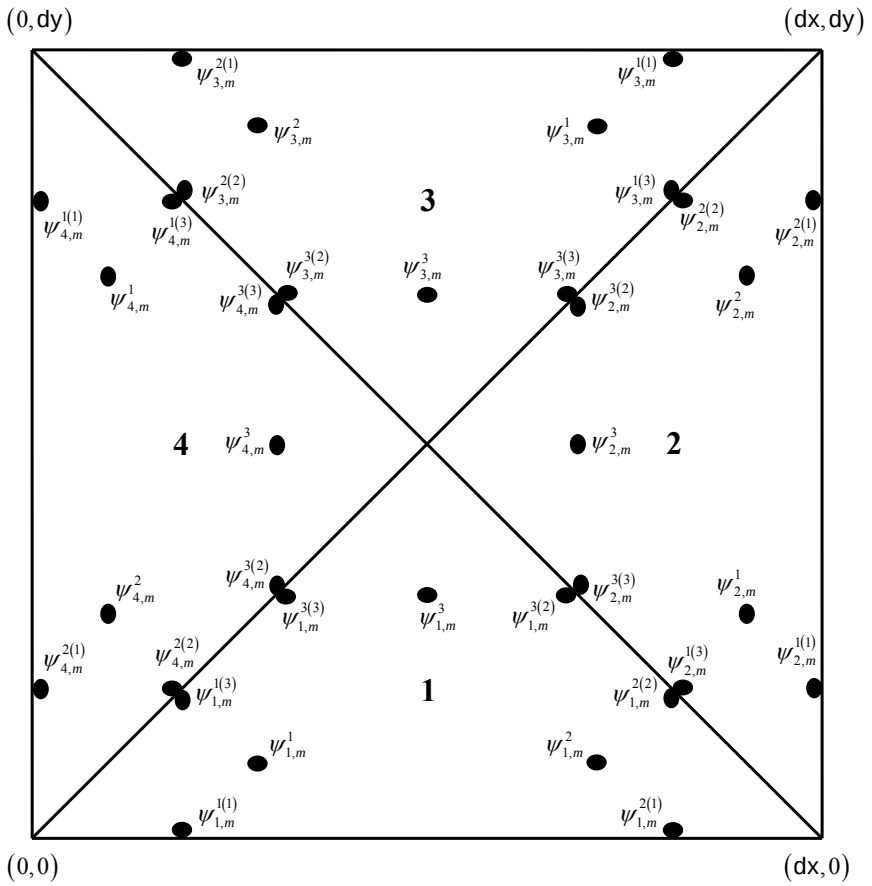


**Figure 1. Four-cell system for the Fourier analysis of cell-wise BJ.**

The equations for the projections of the discrete ordinate angular fluxes onto the linear basis functions of the finite element method, in the four neighboring cells, are grouped together for the discrete ordinates in the four quadrants respectively. An infinite homogeneous medium, in which the four-cell system is periodically repeated, is considered in the Fourier analysis. Therefore, a suitable ansatz must be introduced at the boundaries of the Cartesian element. To fix ideas, the following Fourier ansatz is formulated for the discrete ordinates with cosines $\mu_m < 0$ and $\eta_m > 0$. Analogous expressions are introduced for the discrete ordinates in the remaining quadrants.

Fourier Ansatz $\left(\mu_m < 0, \eta_m > 0\right)$

$$\psi_{1,m}^{i(1)} = \psi_{3,m}^{k(\ell)} \exp\left(-j\lambda_y \sigma \mathsf{dy}\right), \quad i = 1,2;\ k = 2,1; \tag{5}$$

$$\psi_{2,m}^{i(1)} = \psi_{4,m}^{k(\ell)} \exp\left(+j\lambda_x \sigma \mathsf{dx}\right), \quad i = 1,2;\ k = 2,1. \tag{6}$$

In the above equations, $j = \sqrt{-1}$ represents the imaginary unit, $\sigma$ is the macroscopic total cross-section, while $\mathsf{dx}$ ($\mathsf{dy}$) is the width of the Cartesian element in the *x* (*y*) direction. Finally, $\lambda_x$ ($\lambda_y$) is the wave-number of the Fourier modes in the *x* (*y*) direction. The Fourier ansatz accounts for the "lagging" of the incoming angular fluxes on face (1) of both cells 1 and 2 from the

previous iteration. Similar "lagged" boundary conditions are written for the angular fluxes that are incoming on faces that the triangles share in the interior of the Cartesian element.

Substitution of the boundary conditions and of the Fourier ansatz into the original DFEM equations produces, after considerable algebra, the iteration matrix $\mathbf{T}_{BJ}$ for the cell-wise BJ algorithm. Given a certain quadrature order, and values for $\sigma$ and the scattering ratio $c$, the spectral radius $\rho$ of $\mathbf{T}_{BJ}$ is finally obtained as a function of $\mathsf{dx}$ and $\mathsf{dy}$:

$$\rho(\mathsf{dx},\mathsf{dy}) = \max_{\lambda_x,\lambda_y}\left(abs\left(Eig\left(\mathbf{T}_{BJ}\left(\mathsf{dx},\mathsf{dy},\lambda_x,\lambda_y\right)\right)\right)\right). \tag{7}$$

In Fig. 2, we plot the spectral radius as a function of element widths obtained for a level-symmetric $S_4$ quadrature with equal weights, assuming $\sigma = 1$ and $c = 0.5$.

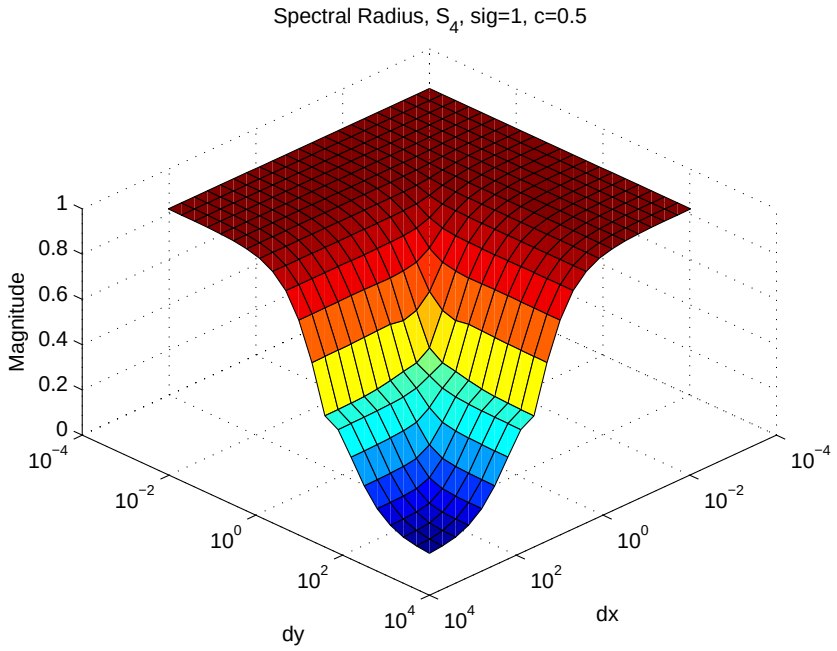


**Figure 2. Fourier analysis for cell-wise BJ: ρ.**

The results in Fig. 2 point to the fact that convergence of cell-wise BJ can degrade for problems containing optically thin cells, even for values of the scattering ratio $c$ less than 1. In fact the spectral radius, as the element widths are decreased, tends to 1 independent from the value of $c$. This is similar to the behavior that was observed for the inexact Parallel Block-Jacobi (PBJ) algorithm in [3]. It appears to be a consequence of the "lagging" of the information on the incoming angular fluxes at the cells' boundaries as the cells are made thinner and become more "strictly coupled". Preconditioning of the PBJ algorithm with Transport Synthetic Acceleration (TSA) proved to be effective in improving the spectral properties of PBJ, especially for optically thin problems, and is envisioned as a possible remedy for the cell-wise BJ algorithm too.

As the computational cells become optically thicker, memory of the information exchanged at the boundaries is lost, and the spectral properties of cell-wise BJ are dominated by the fact that the "full" transport operator is locally inverted on each computational cell. This explains why, as evident in Fig. 2, the spectral radius tends to 0 in the optically thick-cell regime. Hence, for sufficiently optically thick problems the cell-wise BJ algorithm is rapidly convergent even for "diffusive" problems that are scattering dominated with $c$ close to 1; see Fig. 3.

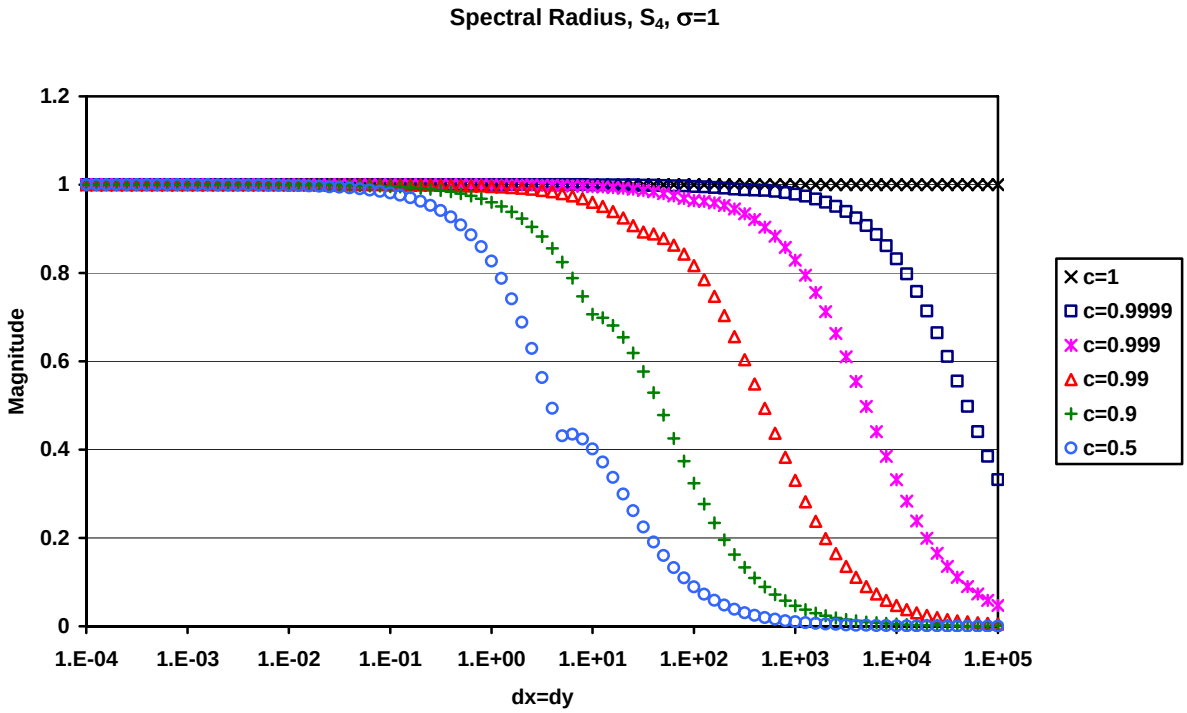


**Figure 3. Spectral radius of cell-wise BJ for various scattering ratios.**

## 2.3. Numerical Results

The predictions from the Fourier analysis for cell-wise BJ have been compared with the numerical results obtained from the implementation of the "Jacobi-Sweeper" in a 2D transport code. For each computational cell in the spatial mesh, the matrix corresponding to the angular ($S_N$) and spatial discretization of the $\left(L_c - SD\right)$ transport operator in Eq. (4) is directly inverted via an LU decomposition.

The results for ρ obtained for a level-symmetric $S_4$ quadrature with equal weights, a unit macroscopic total cross-section and scattering ratios of 0.5 and 0.99 are compared with the Fourier analysis in Tables I and II, respectively.

**Table I. Theoretical and computed ρ of cell-wise BJ for $c=0.5$**

| dx=dy | $10^{-3}$ | $10^{-2}$ | $10^{-1}$ | $10^{0}$ | $10^{+1}$ | $10^{+2}$ | $10^{+3}$ | $10^{+4}$ |
|---|---|---|---|---|---|---|---|---|
| **1×1** | 0.005 | 0.017 | 0.057 | 0.181 | 0.194 | 0.039 | 0.004 | $4\times10^{-4}$ |
| **2×2** | 0.162 | 0.251 | 0.390 | 0.523 | 0.341 | 0.073 | 0.008 | $8\times10^{-4}$ |
| **4×4** | 0.475 | 0.571 | 0.679 | 0.701 | 0.381 | 0.083 | 0.009 | $9\times10^{-4}$ |
| **8×8** | 0.724 | 0.785 | 0.842 | 0.781 | 0.396 | 0.088 | 0.010 | 0.001 |
| **16×16** | 0.864 | 0.897 | 0.923 | 0.812 | 0.400 | 0.089 | 0.010 | 0.001 |
| **32×32** | 0.936 | 0.952 | 0.958 | 0.822 | 0.401 | 0.089 | 0.010 | 0.001 |
| **64×64** | 0.970 | 0.978 | 0.973 | 0.825 | 0.402 | 0.089 | 0.010 | 0.001 |
| **128×128** | 0.986 | 0.990 | 0.978 | 0.826 | 0.402 | 0.089 | 0.010 | 0.001 |
| **Fourier** | **0.999** | **0.998** | **0.981** | **0.827** | **0.402** | **0.089** | **0.010** | **0.001** |

**Table II. Theoretical and computed ρ of cell-wise BJ for $c=0.99$**

| dx=dy | $10^{-3}$ | $10^{-2}$ | $10^{-1}$ | $10^{0}$ | $10^{+1}$ | $10^{+2}$ | $10^{+3}$ | $10^{+4}$ |
|---|---|---|---|---|---|---|---|---|
| **1×1** | 0.007 | 0.024 | 0.085 | 0.327 | 0.759 | 0.718 | 0.237 | 0.032 |
| **2×2** | 0.184 | 0.288 | 0.462 | 0.725 | 0.910 | 0.789 | 0.308 | 0.043 |
| **4×4** | 0.502 | 0.607 | 0.740 | 0.897 | 0.947 | 0.805 | 0.323 | 0.046 |
| **8×8** | 0.742 | 0.808 | 0.889 | 0.965 | 0.957 | 0.813 | 0.328 | 0.047 |
| **16×16** | 0.875 | 0.911 | 0.957 | 0.987 | 0.960 | 0.816 | 0.330 | 0.047 |
| **32×32** | 0.941 | 0.961 | 0.985 | 0.994 | 0.960 | 0.816 | 0.330 | 0.047 |
| **64×64** | 0.973 | 0.984 | 0.995 | 0.995 | 0.960 | 0.816 | 0.330 | 0.047 |
| **128×128** | 0.988 | 0.994 | 0.998 | 0.996 | 0.960 | 0.816 | 0.330 | 0.047 |
| **Fourier** | **1.000** | **1.000** | **0.999** | **0.996** | **0.961** | **0.817** | **0.330** | **0.047** |

To reproduce the conditions of the Fourier analysis, the 2D transport code was used to solve a sequence of Cartesian meshes, with vacuum boundary conditions, characterized by increasing mesh size. Every Cartesian element in the mesh is subdivided into four triangular cells. Hence, the 1×1 mesh corresponds to the four-cell system depicted in Fig. 1. The results shown in Tables I and II can be understood in view of the fact that, while the theoretical spectrum from the Fourier analysis is obtained for an infinite medium, the actual spectrum incorporates the effect of particle leakage at the boundaries of the finite 2D domain. As the mesh size is increased, for a given element width, the effect of leakage is less and less important. Therefore the values obtained from the code are coincident with one another and with the theoretically predicted ρ in the optically thick regime. As the element width is decreased, the effect of leakage becomes dominant and the estimates of the spectral radius obtained with the code depart from the infinite medium value. As expected, though, the actual spectral radius approaches the theoretical value as the number of cells in the mesh is increased, making the overall domain thicker. The theoretical values would ideally be obtained in the limit as the number of cells in the mesh goes to infinity.

## 3. A GLANCE BEYOND THE CELL-WISE BJ PARADIGM

The results discussed in the previous section indicate that convergence of cell-wise BJ can degrade in problems containing optically thin cells. In this section we present preliminary results from the investigation of two alternative approaches, with respect to the cell-wise BJ paradigm, that can result in a faster transition to the optically thick-cell regime. The first approach is resorting to Gauss-Seidel (GS) instead of the BJ algorithm, so that the most up-to-date information available on the incoming angular fluxes is used at a cell's boundary. This approach, namely cell-wise GS, is discussed in Sec. 3.1 for the most favorable case of a single processor, Np = 1. The second approach entails a "clustering" of cells leading from cell-wise (or single-cell) BJ to an *n*-cell BJ, in which the incoming angular fluxes are only "lagged" at the boundaries of the *n*-cell "cluster". Specifically, the case $n=4$ is illustrated in Sec. 3.2.

### 3.1. Fourier Analysis of Cell-Wise GS (Np = 1)

For cell-wise BJ the incoming angular fluxes at all the boundaries of a computational cell are "lagged" from the previous iteration. Therefore, whether a cell boundary is coincident or not with the interface between two different processors, in the parallel implementation of the "Jacobi-Sweeper", has no consequence on the spectral properties of the cell-wise BJ algorithm. Hence, no mention on the number of processors was made either in devising the Fourier analysis for cell-wise BJ or in discussing the results contained in Tables I and II. For the same reason, the order in which the four triangular cells over the Cartesian element depicted in Fig. 1 are swept by the "Jacobi-Sweeper" has no impact on the spectral properties of cell-wise BJ.

Since in the cell-wise GS algorithm the most up-to-date information available on the incoming angular fluxes is used at any of the cell's boundaries, the above circumstances no longer hold true. Under the assumption of a single processor, a Fourier analysis for cell-wise GS can be devised by referring to the system of four triangular cells over a Cartesian element sketched in Fig. 1. We also assume the sweeping sequence 4-1-2-3 for the triangular cells. This implies, for example, that the information on the angular fluxes incoming on cell 1 from cell 4 is already available at $(\ell+1)$ while that from cell 2 is only available at $(\ell)$. To further fix ideas, while Eq. (5) for the Fourier ansatz previously formulated for cell-wise BJ remains the same for cell-wise GS, Eq. (6) needs to be replaced with:

$$\psi_{2,m}^{i(1)} = \psi_{4,m}^{k(\ell+1)} \exp\left(+j\lambda_x \sigma \mathrm{dx}\right), \quad i=1,2;\ k=2,1. \tag{8}$$

Therefore, the cell-wise GS algorithm is based on splitting the $L$ operator into two contributions $L_c^*$ and $L_b^*$ which are different from $L_c$ and $L_b$ for cell-wise BJ, respectively; see Eqs. (3) and (4). Since part of the contributions originally "lagged" from the previous iteration for cell-wise BJ via $L_b$ are attributed to $L_c^*$, it is expected that the iteration operator $\mathbf{T}_{GS}$ for cell-wise GS should display improved spectral properties with respect to $\mathbf{T}_{BJ}$. The latter expectation is verified by the comparison of the spectral radii of cell-wise BJ and GS presented in Fig. 4 for different values of the scattering ratio.

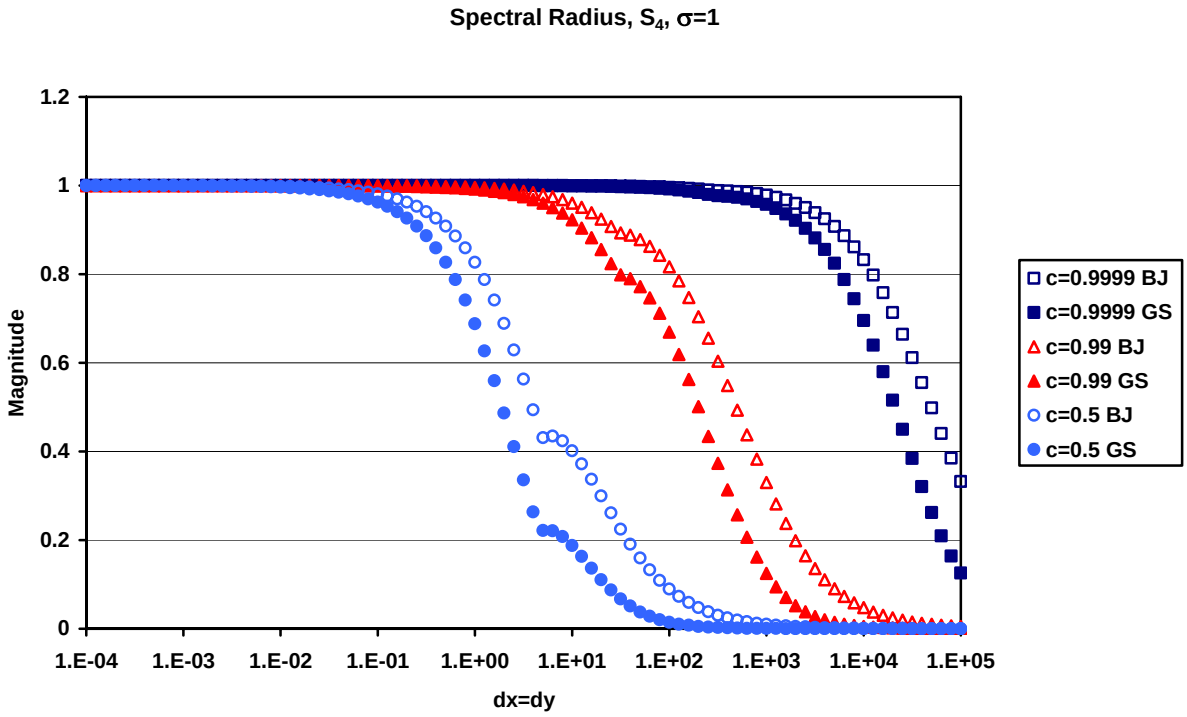


**Figure 4. Spectral radii of cell-wise BJ and GS for various scattering ratios.**

For all the values of *c* attempted the curve for cell-wise GS lies below the corresponding curve for cell-wise BJ, except for sufficiently optically thin problems where both curves approach a value of 1. In particular, cell-wise GS enters the optically thick-cell regime, characterized by a value of ρ vanishing to 0, at a faster rate than cell-wise BJ.

A straightforward way of numerically implementing the cell-wise GS algorithm is obtained by modifying the "Jacobi-Sweeper" in the 2D code. For cell-wise BJ the values of the discrete angular fluxes computed in the previous iteration must be available to compute the updated angular fluxes in the present iteration. Hence, the "Jacobi-Sweeper" makes use of two vectors to store the two sets of discrete variables. The vector containing the old values of the angular fluxes is then overwritten with the new values obtained at the end of the present iteration, before initiating a new iteration. Cell-wise GS is implemented by eliminating the vector containing the old values. A single vector is employed instead that is overwritten as soon as a new value for an angular flux is available. The so implemented "Gauss-Seidel-Sweeper" was used to verify the predictions from the Fourier analysis for cell-wise GS with the 2D transport code. To reproduce the conditions of the Fourier analysis, the code ran on a single processor to solve the sequence of Cartesian meshes, with vacuum boundary conditions, first introduced in Sec. 2.3. The values for ρ predicted by the Fourier analysis for the level-symmetric $S_4$ quadrature, a unit macroscopic total cross-section and scattering ratios of 0.5 and 0.99 are verified by the estimates of ρ obtained from the code in Tables III and IV, respectively.

**Table III. Theoretical and computed ρ of cell-wise GS for $c=0.5$**

| dx=dy | $10^{-3}$ | $10^{-2}$ | $10^{-1}$ | $10^{0}$ | $10^{+1}$ | $10^{+2}$ | $10^{+3}$ | $10^{+4}$ |
|---|---|---|---|---|---|---|---|---|
| **1×1** | $5\times10^{-4}$ | 0.003 | 0.013 | 0.062 | 0.065 | 0.007 | $3\times10^{-4}$ | $2\times10^{-5}$ |
| **2×2** | 0.037 | 0.078 | 0.172 | 0.295 | 0.131 | 0.010 | $4\times10^{-4}$ | $2\times10^{-5}$ |
| **4×4** | 0.231 | 0.333 | 0.469 | 0.503 | 0.168 | 0.013 | $5\times10^{-4}$ | $2\times10^{-5}$ |
| **8×8** | 0.524 | 0.618 | 0.712 | 0.618 | 0.182 | 0.014 | $5\times10^{-4}$ | $2\times10^{-5}$ |
| **16×16** | 0.747 | 0.806 | 0.852 | 0.665 | 0.186 | 0.015 | $5\times10^{-4}$ | $2\times10^{-5}$ |
| **32×32** | 0.875 | 0.907 | 0.919 | 0.681 | 0.187 | 0.015 | $5\times10^{-4}$ | $2\times10^{-5}$ |
| **64×64** | 0.941 | 0.957 | 0.947 | 0.686 | 0.188 | 0.015 | $5\times10^{-4}$ | $2\times10^{-5}$ |
| **128×128** | 0.973 | 0.980 | 0.957 | 0.688 | 0.188 | 0.015 | $5\times10^{-4}$ | $2\times10^{-5}$ |
| **Fourier** | **0.999** | **0.996** | **0.962** | **0.688** | **0.188** | **0.015** | **$5\times10^{-4}$** | **$2\times10^{-5}$** |

**Table IV. Theoretical and computed ρ of cell-wise GS for $c=0.99$**

| dx=dy | $10^{-3}$ | $10^{-2}$ | $10^{-1}$ | $10^{0}$ | $10^{+1}$ | $10^{+2}$ | $10^{+3}$ | $10^{+4}$ |
|---|---|---|---|---|---|---|---|---|
| **1×1** | $8\times10^{-4}$ | 0.004 | 0.022 | 0.146 | 0.587 | 0.528 | 0.080 | 0.004 |
| **2×2** | 0.046 | 0.100 | 0.231 | 0.535 | 0.830 | 0.626 | 0.108 | 0.005 |
| **4×4** | 0.258 | 0.375 | 0.555 | 0.807 | 0.896 | 0.650 | 0.119 | 0.005 |
| **8×8** | 0.552 | 0.655 | 0.791 | 0.931 | 0.916 | 0.664 | 0.123 | 0.005 |
| **16×16** | 0.766 | 0.831 | 0.916 | 0.974 | 0.921 | 0.668 | 0.124 | 0.005 |
| **32×32** | 0.886 | 0.924 | 0.970 | 0.987 | 0.922 | 0.669 | 0.125 | 0.005 |
| **64×64** | 0.947 | 0.970 | 0.990 | 0.991 | 0.923 | 0.670 | 0.125 | 0.005 |
| **128×128** | 0.976 | 0.988 | 0.996 | 0.992 | 0.923 | 0.670 | 0.125 | 0.005 |
| **Fourier** | **1.000** | **0.999** | **0.999** | **0.992** | **0.923** | **0.670** | **0.125** | **0.005** |

The dependence of the spectral properties of cell-wise GS on Np is due to the fact that the information on the angular fluxes incoming on an interface between two adjacent processors, available in the present iteration, was communicated at the end of the previous iteration. As a simple illustration of the impact of an interface on the Fourier analysis for cell-wise GS, imagine that face (1) of cell 2, in Fig. 1, lies at the interface between two different processors. Under this assumption, for example, Eq. (8) is no longer valid and must be replaced with Eq. (6). Part of the cell's interior contribution exerted via $L_c^*$ is therefore reattributed back to $L_b^*$. This leads in turn to a new splitting of the $L$ operator and to a different iteration operator, $\mathbf{T}_{GS1Int}$, whose spectral properties are expected to be intermediate between those of $\mathbf{T}_{GS}$ and $\mathbf{T}_{BJ}$, respectively. This reasoning helps understanding the results presented in Fig. 5 for $c=0.5$. The GS and BJ curves are the same as in Fig. 4. The curve for two interfaces was obtained for the case in which both face (1) of cell 2 and face (1) of cell 3 coincide with the interface between different processors.

Further research is needed in order to possibly tie the parameter Np into the Fourier analysis for cell-wise GS. It is expected, though, that the curves obtained from this more refined analysis for a given $c$ would have to lie somewhere in between the GS curve and the BJ curve; see Fig. 5.

The former curve is the lower envelope obtained for the most favorable case of Np = 1. The latter is the upper envelope and is equivalent to cell-wise GS for the worst case of Np = Nc, where Nc is the number of cells in the mesh.

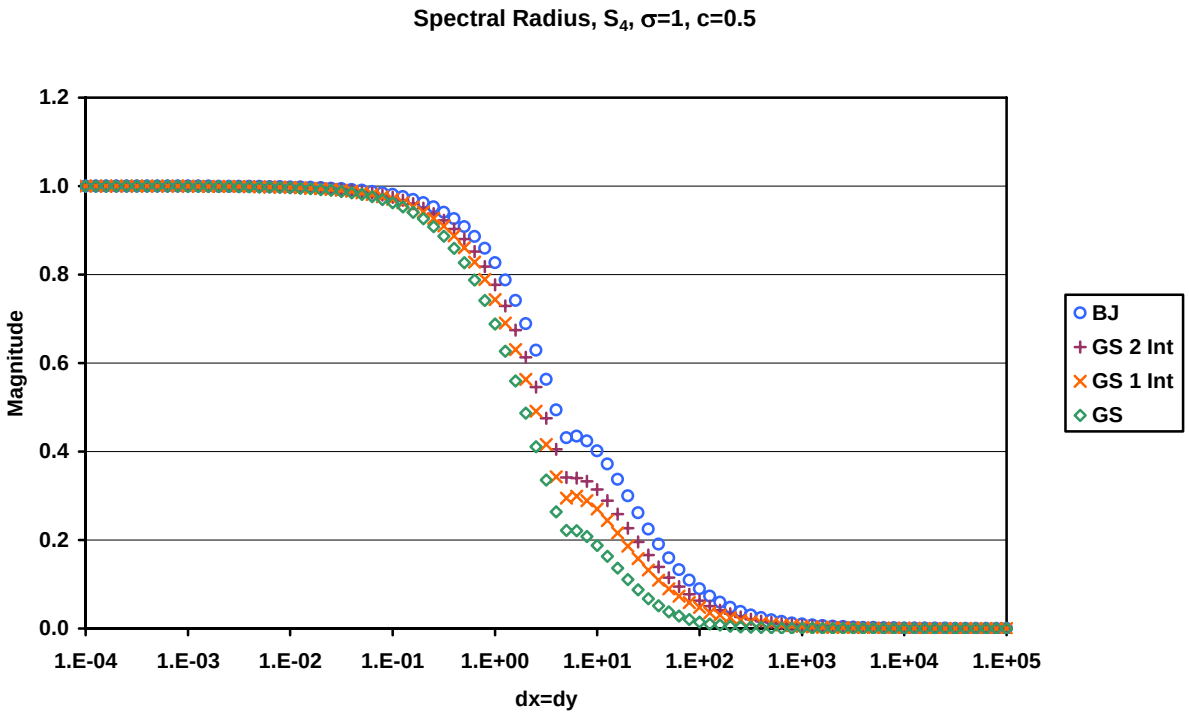


**Figure 5. Effect of processor interface on the spectral properties of cell-wise GS.**

### 3.2. Fourier Analysis of *n*-cell BJ (*n* = 4)

To illustrate the intuition behind applying the BJ algorithm to "clusters" of cells, as opposed to a single cell in order to improve its spectral properties, it is convenient to refer to the following ideal situation. Assume the discretized computational domain of a transport problem characterized, for ease of reasoning, by explicit boundary conditions is given. Imagine then that the BJ splitting is applied to the entire domain. If one were indeed able to construct $L_c$ (domain's interior) and $L_b$ (domain's boundaries) then inversion of $(L_c - SD)$ on the known incoming boundary fluxes and fixed source contributions would directly produce the solution to the transport problem, without the need for an iterative procedure. Consequently, the spectral radius for the BJ operator would be 0, independent from the optical properties of the computational cells comprising the domain. We conjecture then that an *n*-cell iterative BJ algorithm, in which the BJ splitting is applied to a "cluster" of *n* cells, should be characterized by spectral properties that are intermediate between the ideal case considered above ($n$ = Nc) and cell-wise BJ ($n$ = 1).

The system of four triangular cells over the Cartesian element depicted in Fig. 1 is used to test the above conjecture for $n$ = 4. Specifically, the Fourier analysis originally devised for cell-wise

BJ is modified by assuming that the incoming angular fluxes are only "lagged" at the boundaries of the 4-cell "cluster", not at the cells' boundaries that lie inside the "cluster". In other words, the discrete angular fluxes for the four cells as a whole are computed altogether simultaneously rather than one cell at a time. The curves for the spectral radii of cell-wise BJ and 4-cell BJ are compared in Fig. 6 for different values of the scattering ratio.

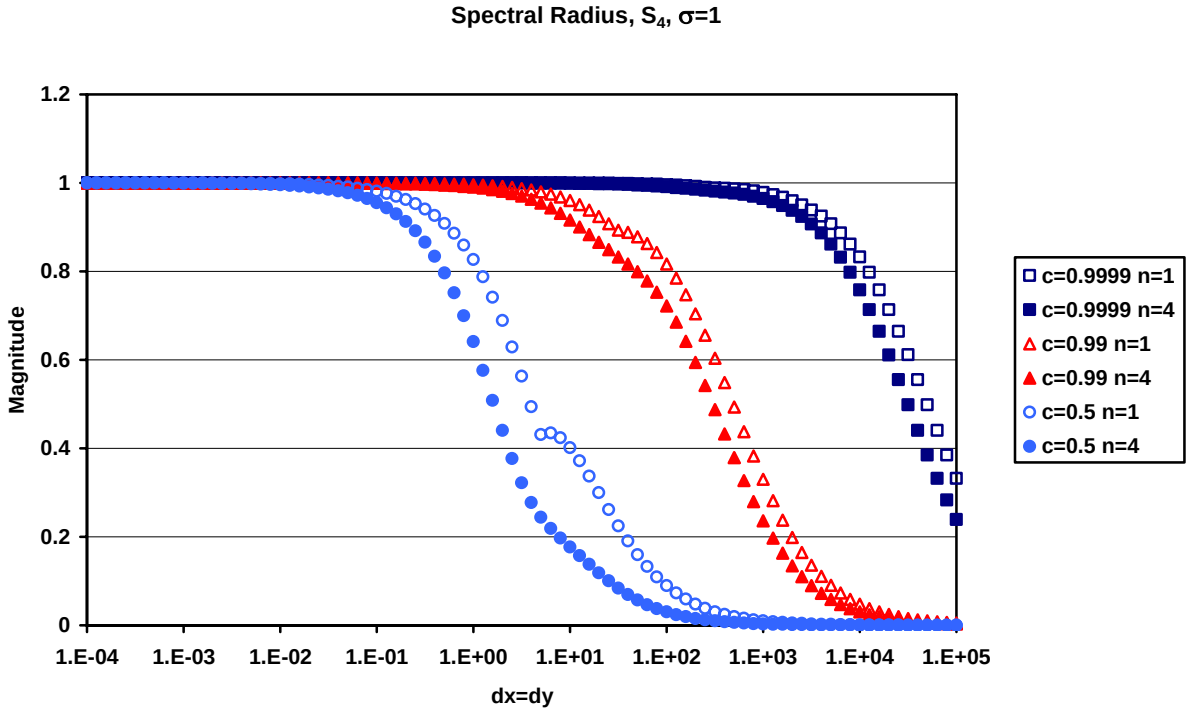


**Figure 6. Spectral radii of cell-wise BJ and 4-cell BJ for various scattering ratios.**

For all the values of $c$ attempted the results presented in Fig. 6 verify the conjecture formulated at the beginning of this section. Specifically, 4-cell BJ is characterized by a faster transition to the optically thick-cell regime than cell-wise BJ. Also, it appears that the "clustering" has a nice "smoothing" effect, especially for $c = 0.5$, on the curves for the spectral radius in the transition region. We presently lack a thorough understanding of the origin of the "peaks" displayed by the curves for the spectral radii of BJ and GS in this region.

Further research is required to fully understand the potential advantages of the $n$-cell BJ strategy. From a numerical implementation stand-point, the improved spectral properties of $n$-cell BJ with respect to cell-wise BJ may come at the price of identifying an optimal "clustering strategy" for the computational mesh, especially for unstructured meshes. For example, assuming $n = 4$ for an unstructured triangular mesh, in which order should four triangles at a time be "clustered" together in order to ensure optimal spectral properties and performance of the algorithm? Also, the computational burden and the storage requirements associated with the inversion of the $n$-cell BJ operator scale with $n$. While the high computational burden makes such algorithm appealing for advanced heterogeneous computing architectures, the storage requirements may impose a significant limitation on $n$. Finally, it is desired to study the impact on BJ's spectral properties of coupling the "clustering" with overlap strategies in which a cell is shared by multiple "clusters".

## 4. CONCLUSIONS

A Fourier analysis has been implemented for the cell-wise Block-Jacobi (BJ) algorithm. The results of the Fourier analysis show that cell-wise BJ is rapidly convergent, with a spectral radius vanishing to 0, in problems containing optically thick cells. Interestingly, this feature holds also for scattering dominated problems ($c \sim 1$). It is well known that for systems containing "diffusive" spatial regions that are optically thick and scattering dominated the traditional Source Iteration (SI) algorithm converges slowly. Since many important applied problems do contain "diffusive" regions it has long been desired to accelerate the iterative convergence of SI. The cell-wise BJ algorithm can overcome such limitations at the higher computational cost resulting from its numerical implementation. In this connection, cell-wise BJ could be a suitable algorithm for deterministic transport computations on the parallel, advanced heterogeneous computing architectures that are gradually becoming available to the computational transport community.

In the opposite limit of optically thin-cells, the spectral radius of cell-wise BJ tends to a value of 1, independent from the scattering ratio $c$. Hence, convergence of cell-wise BJ can degrade in problems containing optically thin cells and preconditioning of the basic iterative scheme, to be investigated in future research, may be needed to improve its spectral properties in this regime. In this paper we presented preliminary results for two non-accelerated iterative schemes, alternative to cell-wise BJ, that result in a faster transition to the optically thick-cell regime. The first iterative scheme is based on Gauss-Seidel (GS) instead of the BJ algorithm, so that the most up-to-date information available on the incoming angular fluxes is used at a cell's boundary. The second iterative scheme exploits a "clustering" of cells, leading from cell-wise (or single-cell) BJ to an $n$-cell BJ, in which the incoming angular fluxes are only "lagged" at the boundaries of the $n$-cell "cluster". For the two alternative schemes the improvement in spectral properties with respect to cell-wise BJ comes at the expense of introducing a suitable cell-ordering either in the "sweeping" or in the "clustering" of the computational cells in the mesh, respectively. Also, the spectral properties of GS depend on the number of processors used in the parallel computation.

## ACKNOWLEDGMENTS

This information has been authored by employees of the Los Alamos National Security, LLC (LANS) operator of Los Alamos National Laboratory under contract No DE-AC52-06NA25396 with the U.S. Department of Energy.

## REFERENCES

1. C. H. Crawford, P. Henning, M. Kistler, C. Wright, "Accelerating Computing with the Cell Broadband Engine Processor," *Proceedings of the 2008 Conference on Computing Frontiers*, Ischia, Italy, May 5-7, 2008, pp. 3-11 (2008).
2. M. L. Adams, "Discontinuous Finite Element Transport Solutions in Thick Diffusive Problems," *Nucl. Sci. Eng.*, **137**, pp. 298-333 (2001).
3. M. Rosa, J. S. Warsa, J. H. Chang, "Fourier Analysis of Parallel Block-Jacobi Splitting with Transport Synthetic Acceleration in Two-Dimensional Geometry," *Proceedings of the International Topical Meeting M&C 2007*, Monterey, CA, Apr. 15-19, 2007, on CD-ROM, ANS, LaGrange Park, IL (2007).